WILEY

IET-Wiley Virtual Symposium on Renewable Energy 2022

Digital and flexible control and operation of transmission and distribution grids for renewable power systems.

September 13 2022

Research conducted at institutions in Germany has led to exciting advances in the areas of renewable energy. This free virtual symposium supported by two of the IET's flagship open access journals *IET Renewable Power Generation (RPG)* and *IET Generation, Transmission & Distribution (GTD)* will be free to attend. It will provide a forum for researchers based in Germany to highlight their research and will celebrate the capacity for renewable energy research to engineer a better world.

Session Topics Include:

- Power Flow Control for efficient Transmission Grids
- Digitalization of Power Systems
- Flexibility in Power Systems
- Smart Distribution Grids

Register free today

The Institution of Engineering and Technology

Received: 11 January 2022 | Revised: 27 March 2022 | Accepted: 25 April 2022

IET Generation, Transmission & Distribution

DOI: 10.1049/gtd2.12567

The Institution of Engineering and Technology WILEY

ORIGINAL RESEARCH

Modified unified power flow controller for medium voltage distribution networks

Mohamed A. Abdelrahman[1,2] | **Peng Yang**[1] | **Wenlong Ming**[1] | **Jianzhong Wu**[1] | **Nick Jenkins**[1]

[1]Department of Electrical and Electronic Engineering, School of Engineering, Cardiff University, Cardiff, UK

[2]Department of Electrical Power and Machines, Faculty of Engineering, Helwan University, Helwan, Egypt

Correspondence
Wenlong Ming, Room E/2.13, Queen's Buildings, 5 The Parade, Newport Road, Cardiff CF24 3AA, UK.
Email: mingw@cardiff.ac.uk

Funding information
Engineering and Physical Sciences Research Council, U.K., Grant/Award Number: EP/T021969/1

Abstract

A conventional unified power flow controllers (UPFCs) can provide power flow control and voltage regulation in medium voltage (MV) distribution networks using partially rated converters. However, one of the main challenges of using the conventional UPFC is the unique design of the series interfacing transformer. This paper investigates a modified topology of a UPFC suitable for MV distribution networks. The modified UPFC does not need an interfacing series transformer. Hence, it offers a smaller size, lighter weight, and less cost than the conventional UPFC. It consists of single-phase back-to-back series and shunt voltage source converters. The series converters are connected to a distribution network without a series transformer, while the shunt converters are interfaced using a three-phase shunt transformer. The power ratings of the series and shunt converters were investigated considering a distribution network with a low X/R ratio. The modified UPFC was modelled in MATLAB Simulink and was connected to a two-busbar distribution network and the enhanced IEEE 33-bus distribution network. The results showed the ability of the modified UPFC to independently control active and reactive power in a distribution feeder by processing a fraction of the power transfer through the converters.

1 | INTRODUCTION

Decarbonisation of the energy sector includes more low carbon technologies (LCTs) such as solar photovoltaic (PV) systems and wind turbines [1]. The main challenges limiting more of LCTs, that will often be connected to distribution networks, are voltage rise and network congestion [2]. At present, the operation of distribution networks is passive. New devices are required to provide distribution network operators with the means of controlling the power flow and improving the utilisation of existing distribution networks.

In the UK, the accumulated capacity of solar photovoltaics generation connected to the distribution networks has increased to 12.9 GW and wind generation to 5.7 GW [3]. The growth in renewable generation has increased the supply of green electricity. Still, it has imposed operational challenges as renewable energy is intermittent, and the output does not necessarily coincide with the local demand. The distribution networks should be adapted to accommodate more of renewable generation at the lowest cost and maximum flexibility [4].

Power electronic devices (e.g. voltage source converters [VSCs]) can be used to provide power flow control in medium voltage (MV) distribution networks, similar to the well-established flexible AC transmission systems (FACTs) and MV motor drive systems. This is demonstrated by several projects that have been trialling new configurations and arrangements of power electronic converters in MV distribution networks [5–10].

Back-to-back (B2B) connection of VSCs is the most common configuration of power electronic devices in MV distribution networks that are interfaced to distribution networks using line-frequency interfacing transformers. Several studies were conducted to quantify the benefits of installing fully rated B2B VSCs in MV distribution networks [11, 12]. The fully rated B2B

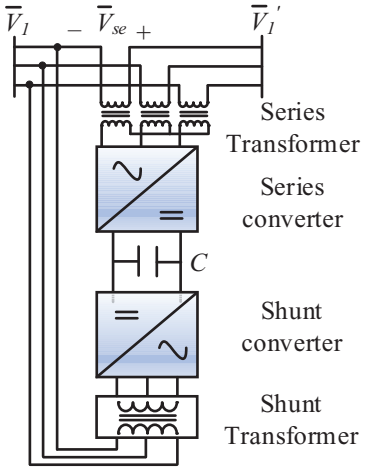

FIGURE 1 Circuit diagram of a conventional UPFC in MV distribution networks

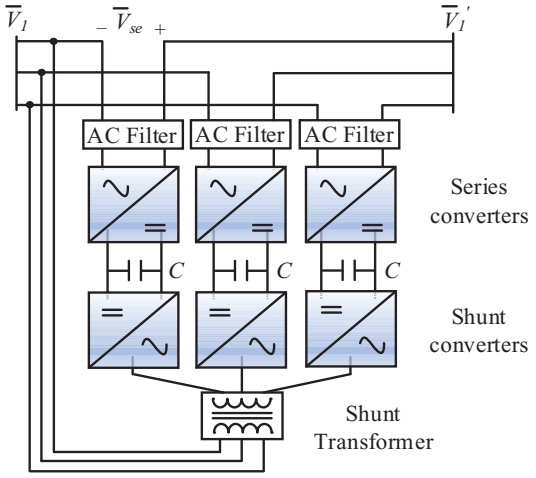

FIGURE 2 Circuit diagram of the modified UPFC in MV distribution networks

VSCs provided power flow control and increased the distributed generators (DGs) hosting capacity of distribution networks [13, 14].

Despite the benefits of installing B2B VSCs, they have not been widely deployed in MV distribution networks, as they are expensive. The cost and size of the fully rated converters and interfacing transformers account for the lack of applications of fully rated B2B VSCs in MV distribution networks.

The series connection of VSCs is an alternative solution to control power flow in distribution networks similar to the well-established unified power flow controller (UPFC), that has been demonstrated in some transmission systems [15–17]. Figure 1 shows a conventional UPFC for applications in MV distribution networks.

In contrast to fully rated B2B VSCs, the series connection of a UPFC offers a solution with partially rated converters and interfacing transformers that reduce its size, weight, and total cost. For example, an 11 kV/400 V, 2 MVA shunt transformer has a size and weight of 5.5 m^3 and 4500 kg. These are only 1.8 m^3 and 1600 kg for a 0.5 MVA shunt transformer of the same voltage rating [18, 19].

One of the main challenges of using a conventional UPFC is the series interfacing transformer. It has unique design characteristics such as (1) a small capacity, (2) the network-side windings are fully insulated and must withstand the network short-circuit current, and (3) the magnetic core has an over-excitation tolerance [20].

This paper investigates a modified topology of a UPFC in MV distribution networks. Figure 2 shows a schematic diagram of the modified UPFC. It can provide power flow control similar to a UPFC without an interfacing series transformer. Hence, it offers a smaller size and less cost. The removal of the series transformer is also adopted in the soft power bridge (SPB) device being trialled by the UK Power Networks project entitled 'Active Response to Distribution Network Constraints' [21], indicating business benefits of removing this part.

The series connection of the modified UPFC is performed using three separate single-phase converters directly connected in series to an MV distribution network instead of a three-phase converter interfaced using a three-phase series transformer in a UPFC. The modified UPFC has three separate DC-link buses. The shunt converters are connected B2B to the series converters, and they are interfaced to a distribution network using a three-phase interfacing shunt transformer. The shunt converters of the modified UPFC can be either single-phase or three-phase converters. In this paper, single-phase shunt converters were used. Three-phase converters require smaller DC-link capacitance, though they require more IGBT modules and a more complex three-phase multi-winding shunt transformer.

The single-phase converters of the modified UPFC were built using a three-level neutral-point-clamped (NPC) topology. The three-level topology reduces the blocking voltage of the insulated gate bipolar transistors (IGBTs) and provides AC voltage with lower harmonic distortion compared to a two-level topology [22]. It has also been used for MV motor drive applications (e.g. GE MV7000) [23].

Power flow equations were derived for a simple two-busbar distribution network with a modified UPFC connected to a distribution feeder with a low X/R ratio. The operating principles of the modified UPFC were presented and procedures for sizing the series and shunt converters were developed. Proportional-resonant (PR) controllers were used to operate the single-phase series and shunt VSCs in power flow control mode. The series converters operated in the P–Q control scheme and the shunt converters in the V_{dc}–Q control scheme.

Step changes of active and reactive power and power flow reversal were performed to test the performance of the modified UPFC model connected to a two-busbar distribution network and the enhanced IEEE 33-bus distribution network.

2 | MODIFIED UPFC IN MV DISTRIBUTION NETWORKS

Figure 3 shows the equivalent circuit of the modified UPFC in a two-busbar distribution network. In such MV network, the

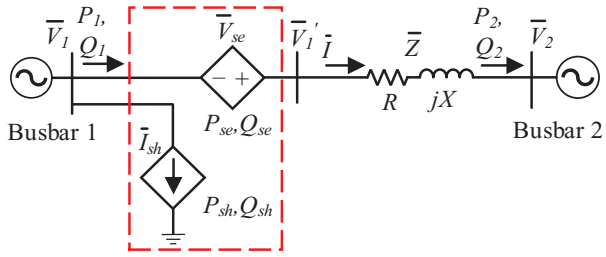

FIGURE 3 Equivalent circuit of the modified UPFC

distribution feeder has low X/R ratio. Therefore, it is represented by a series impedance $\bar{Z}$ where $|\bar{Z}| = \sqrt{R^2 + X^2}$ and $\theta = \tan^{-1}(X/R)$. The series converter is modelled as a controlled voltage source and the shunt converter as a controlled current source.

The series converter injects a controllable voltage $\overline{V}_{se} = |\overline{V}_{se}|\angle\rho$ where $|\overline{V}_{se}| = \sqrt{V_{d,se}{}^2 + V_{q,se}{}^2}$ and $\tan\rho = V_{q,se}/V_{d,se}$. Voltage $\overline{V}_{se}$ is added to voltage $\overline{V}_1$ making the resultant voltage $\overline{V}_1{}' = |\overline{V}_1{}'|\angle\delta_s$ whose magnitude and power angle is controlled to achieve the target active and reactive power P_2 and Q_2. Figure 4 shows the phasor diagram developed using the equivalent circuit in Figure 3 to explain the role of the series converter.

Current $\overline{I} = |\overline{I}|\angle\phi$ flows through the series converter results in active and reactive power exchange (P_{se},Q_{se}) with the connected AC network. Only the active power P_{se} flows through the DC link.

The shunt converter regulates current $\overline{I}_{sh} = I_{sh,d} + jI_{sh,q}$, where $I_{sh,d}$ and $I_{sh,q}$ are the active and reactive current components of $\overline{I}_{sh}$. $I_{sh,d}$ is determined by the requirement of balancing the active power P_{se} of the series converter. $I_{sh,q}$ can be set to achieve a reference voltage or a reference reactive power (i.e. provide voltage regulation of $\overline{V}_1$) within the power capacity of the converter.

The voltage $\overline{V}_1{}'$ and current $\overline{I}$ are o.btained, as in (1).

$$\begin{cases} \overline{V}_1{}' = \overline{V}_1 + \overline{V}_{se} \\ \overline{I} = \dfrac{\overline{V}_1{}' - \overline{V}_2}{|\overline{Z}|\angle\theta} \end{cases} \tag{1}$$

The apparent power $\overline{S}_2$ at busbar 2 is given, as in (2).

$$\overline{S}_2 = \overline{V}_2 \cdot \overline{I}^* = \overline{V}_2 \cdot \left(\frac{\overline{V'}_1 - \overline{V}_2}{|\overline{Z}|\ \angle\theta} \right)^* = P_2 + j\,Q_2 \tag{2}$$

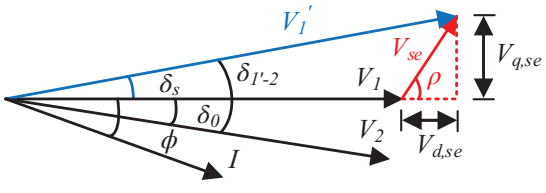

FIGURE 4 Phasor diagram explaining the role of the series converter

Using (2), the active and reactive power (P_2, Q_2) at busbar 2 are given, as in (3).

$$\begin{cases} P_2 = \underbrace{\dfrac{|\overline{V}_1| \times |\overline{V}_2|}{|\overline{Z}|}\cos(\delta_0 + \theta) - \dfrac{|\overline{V}_2|^2}{|\overline{Z}|}\cos\theta}_{\textit{Uncompensated active power}} \\ \quad + \underbrace{\dfrac{|\overline{V}_2| \times |\overline{V}_{se}|}{|\overline{Z}|}\cos(\delta_0 + \theta - \rho)}_{\textit{Controllable active power}} \\ Q_2 = \underbrace{\dfrac{|\overline{V}_1| \times |\overline{V}_2|}{|\overline{Z}|}\sin(\delta_0 + \theta) - \dfrac{|\overline{V}_2|^2}{|\overline{Z}|}\sin\theta}_{\textit{Uncompensated reactive power}} \\ \quad + \underbrace{\dfrac{|\overline{V}_2| \times |\overline{V}_{se}|}{|\overline{Z}|}\sin(\delta_0 + \theta - \rho)}_{\textit{Controllable reactive power}} \end{cases} \tag{3}$$

Equation (3) shows that $\overline{V}_{se}$ affects both P_2 and Q_2. However, if the series converters are deactivated (i.e. $\overline{V}_{se} = 0$), the uncompensated active and reactive power $P_2{}'$ and $Q_2{}'$ are given, as in (4).

$$\begin{cases} P_2{}' = \dfrac{|\overline{V}_1| \times |\overline{V}_2|}{|\overline{Z}|}\cos(\delta_0 + \theta) - \dfrac{|\overline{V}_2|^2}{|\overline{Z}|}\cos\theta \\ Q_2{}' = \dfrac{|\overline{V}_1| \times |\overline{V}_2|}{|\overline{Z}|}\sin(\delta_0 + \theta) - \dfrac{|\overline{V}_2|^2}{|\overline{Z}|}\sin\theta \end{cases} \tag{4}$$

The difference between (3) and (4) is the controllable active and reactive power P_c and Q_c of the modified UPFC (i.e. $P_c = P_2 - P_2{}'$ and $Q_c = Q_2 - Q_2{}'$). P_c and Q_c are given, as in (5).

$$\begin{cases} P_c = \dfrac{|\overline{V}_2 \cdot \overline{V}_{se}|}{Z}\cos(\delta_0 + \theta - \rho) \\ Q_c = \dfrac{|\overline{V}_2 \cdot \overline{V}_{se}|}{Z}\sin(\delta_0 + \theta - \rho) \end{cases} \tag{5}$$

Further simplifying (5) yields an expression of $\overline{V}_{se}$, as in (6).

$$|\overline{V}_{se}| = \frac{|\overline{Z}|}{|\overline{V}_2|}\sqrt{P_c^2 + Q_c{}^2}\ , \rho = (\delta_0 + \theta - \tan^{-1}(\frac{Q_c}{P_c})) \tag{6}$$

Equation (6) shows that $|\overline{V}_{se}|$ is a function of $|\overline{Z}|$, P_c, Q_c and $|\overline{V}_2|$.

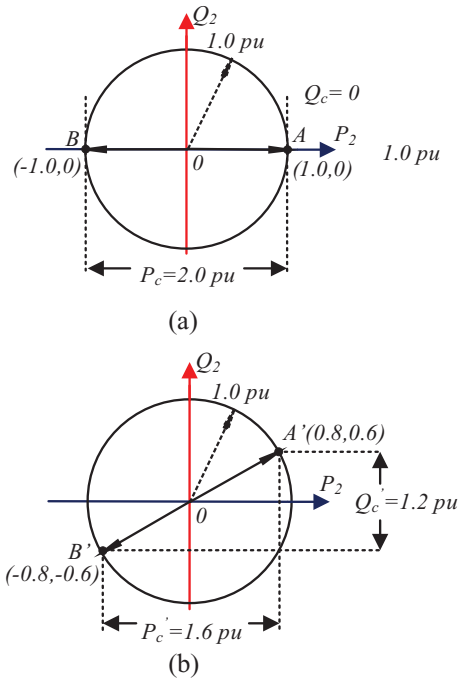

FIGURE 5 PQ diagrams of power transfer showing controllable active and reactive power when power flow reversal occurs; (a) from A to B, and (b) from A′ to B′

3 | POWER RATINGS OF THE SERIES AND SHUNT CONVERTERS

The series and the shunt converters' power ratings must fulfil the maximum apparent power $|\overline{S}_{se}|$ and $|\overline{S}_{sh}|$ exchanged between the converters and the connected AC network such as $|\overline{V}_{se}| \cdot |\overline{I}| \leq |\overline{S}_{se}|$ and $|\overline{V}_1| \cdot |\overline{I}_{sh}| \leq |\overline{S}_{sh}|$. The active power exchanged by the series and shunt converters is equal (i.e. $P_{se} = P_{sh}$), assuming lossless converters. The series and shunt converters independently exchange reactive power with the network.

3.1 | Series converter

The power rating of the series converter can be estimated by calculating voltage $|\overline{V}_{se}|$ using (6). Note that $|\overline{V}_{se}|$ is advantageously smaller in MV distribution networks than transmission networks due to the smaller impedance.

The controllable power $P_c$and Q_c depend on the operating range of the modified UPFC. Figure 5 shows the PQ diagrams of the power transferred through an AC distribution feeder and is used to present two examples for the controllable power P_c and Q_c when $\sqrt{P_c^2 + Q_c^2}$ is maximum. Figure 5a shows power flow reversal occurs from point A (1.0 pu, 0 pu) to point B (−1.0 pu, 0 pu), where the per-unit values in each bracket are the active and reactive power. Figure 5b shows power flow reversal occurs from point A′ (0.8 pu, 0.6 pu) to point B′ (′0.8 pu, ′0.6 pu). In both cases, $\sqrt{P_c^2 + Q_c^2}$ has a maximum value of 2.0 pu.

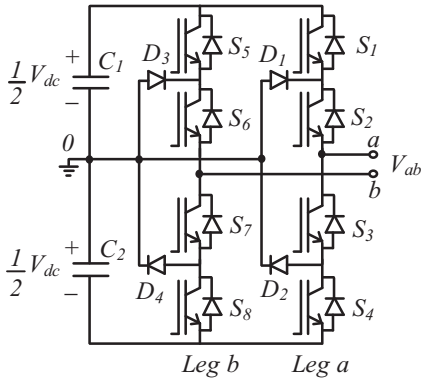

FIGURE 6 A single-phase three-level full-bridge NPC converter

Assuming $|\overline{V}_2|$ is 0.95 pu, and $|\overline{Z}|$ ranges between 5% and 10%. Using (6), $|\overline{V}_{se}|$ ranges between 0.105 pu and 0.210 pu. As current $|\overline{I}|$ is 1.0 pu, the apparent power of the series converter $|\overline{S}_{se}|$ ranges between 0.105 pu and 0.210 pu.

3.2 | Shunt converter

The power rating of the shunt converter can be estimated by calculating current $|\overline{I}_{sh}|$ whose direct component $I_{sh,d}$ is proportional to the active power P_{sh}, and quadrature component $I_{sh,q}$ to the reactive power Q_{sh} (i.e. $P_{sh} \propto I_{sh,d}$ and $Q_{sh} \propto I_{sh,q}$).

The power rating of the shunt converter must be at least as large as the active power of the series converter. Assuming the series converter operates at full load and unity power factor, the apparent power of the shunt converter is at least equal to the apparent power of the series converter (i.e. $|\overline{S}_{se}| = |\overline{S}_{sh}|$). In this case, the minimum apparent power of the shunt converter ranges between 0.105 pu and 0.210 pu. Additional capacity is required to provide the reactive current needed for voltage regulation.

4 | CONTROL SCHEME

4.1 | SPWM of a single-phase three-level NPC converter

Figure 6 shows the circuit configuration of a single-phase three-level full-bridge NPC converter. The DC voltage V_{dc} is split into three voltage levels $+1/2V_{dc}$, $-1/2V_{dc}$ and zero by the two series-connected capacitors.

Sinusoidal pulse-width modulation (SPWM) was used to generate the gate signals ($S_1 \rightarrow S_8$) for the IGBTs. Figure 7 shows the operating principles of the SPWM for a single-phase three-level full-bridge NPC converter. Two modulating signals, m_a and m_b, are compared with two triangle signals C_1 and C_2, to generate the gate signals ($S_1 \rightarrow S_4$) and ($S_5 \rightarrow S_8$) of leg-a and leg-b, as shown in Figure 7a [24]. The output voltages V_{a0} of leg-a and V_{b0} of leg-b are shown in Figure 7b. The output voltage

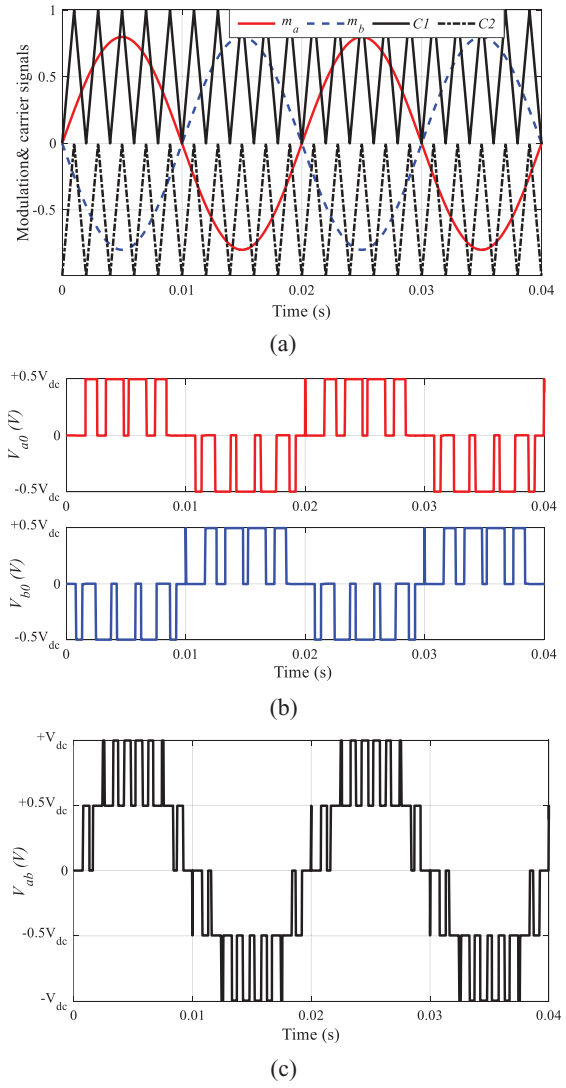

FIGURE 7 Operating principles of SPWM; (a) reference and carrier signals, (b) voltage of leg a and b, and (c) output voltage

V_{ab} of the single-phase three-level NPC converter is shown in Figure 7c.

4.2 | Power flow control mode

The modified UPFC was controlled to operate in power flow control mode. The series converters operate in P–Q control scheme to regulate active and reactive power of a distribution feeder. The shunt converters operate in V_{dc}–Q control scheme to maintain constant DC voltages across the DC-link buses and provide/absorb reactive power Q_{sh} at the point of connection (e.g. busbar $\overline{V}_1$).

PI controllers are not well suited for single-phase converters. They require computational effort to provide an orthogonal component (i.e. β axis component) of voltages and currents in the $\alpha\beta$ frame [25]. An alternative to synchronous dq frame PI controllers is stationary frame PR controllers. A PR controller combines a proportional gain and a resonant path tuned at the desired frequency [26]. The basic transfer function of a PR controller $G_c(s)$ is given, as in (7).

$$G_c(s) = K_p + \frac{K_i}{s^2 + w_r s + w_0{}^2} \tag{7}$$

where K_p and K_i are the proportional and integral gains, w_r and w_0 are the resonant cut-off frequency and the resonant target frequency [27].

Figure 8 shows the control loops of the modified UPFC. Figure 8a shows the control loops of the series converter. The control of P_1 and Q_1 is achieved by regulating current $\overline{I}$ of the distribution feeder. The current $\overline{I}$ is regulated by injecting the corresponding voltage $\overline{V}_{se}$. The reference active and reactive power $P_1{}^*$ and $Q_1{}^*$ are transformed into dq current components $I_d{}^* = P_1{}^*/1.5V_d$ and $I_q{}^* = -Q_1{}^*/1.5V_d$, where V_d is the direct component of voltage $\overline{V}_1$. The dq current components $I_d{}^*$ and $I_q{}^*$ are transformed into $\alpha\beta$ current components $I_\alpha{}^*$ and $I_\beta{}^*$ using dq–$\alpha\beta$ transformation. A phase-locked loop (PLL) is used to generate the phase information θ of $\overline{V}_1$. Two separate anti-windup PR controllers are used to regulate the $\alpha\beta$ current components I_α and I_β of the current $\overline{I}$ [28]. The output of the PR controllers is the modulating signals $m_{\alpha,se}$ and $m_{\beta,se}$ in $\alpha\beta$ frame, and they are converted into $m_{se,abc}$ in abc frame using $\alpha\beta$–abc transformation. SPWM is used to generate the gate signals ($S_{1,abc} \rightarrow S_{8,abc}$) to drive the IGBTs of the three single-phase series converters. Thus, the series converters generate the voltages ($V_{se,a}$, $V_{se,b}$, and $V_{se,c}$) that maintain the errors between the reference and measured currents ($I_\alpha{}^* - I_\alpha$) and ($I_\beta{}^* - I_\beta$) minimal. Hence, P_1 and Q_1 will be maintained close to $P_1{}^*$ and $Q_1{}^*$.

The DC-link voltage constrains the maximum series voltage. The maximum series voltage should be calculated first depending on the feeder's impedance and the controllable power, then the DC-link voltage is determined. The anti-windup controllers in Figure 8 ensure that the controllers' outputs do not exceed the modulation limits. Current limiters for $I_d{}^*$ and $I_q{}^*$ are inserted in Figure 8a to limit overcurrent during disturbances.

Figure 8b shows three separate control loops that are used to control the three single-phase shunt converters. $V_{dc}{}^*$ and $Q_{sh}{}^*$ are the reference DC voltage and reactive power of the shunt converters. The error signals of the DC voltages $\Delta V_{dc,a}$, $\Delta V_{dc,b}$, and $\Delta V_{dc,c}$ and of the reactive power $\Delta Q_{sh,a}$, $\Delta Q_{sh,b}$, and $\Delta Q_{sh,c}$ are manipulated using PI controllers to generate the reference direct and quadrature current components $I_{d,a}{}^* + jI_{q,a}{}^*$, $I_{d,b}{}^* + jI_{q,b}{}^*$, and $I_{d,c}{}^* + jI_{q,c}{}^*$ of the single-phase shunt converters. The reference current of each single-phase shunt converter is determined as given in (8).

$$i_{abc}{}^*(t) = I_{d,abc}{}^* \sin(\theta_{abc}) + I_{q,abc}{}^* \cos(\theta_{abc}) \tag{8}$$

The PR controllers track the reference currents $i_{abc}{}^*(t)$ and generate the modulating signals $m_{sh,abc}$ before being converted into PWM signals to drive the IGBTs.

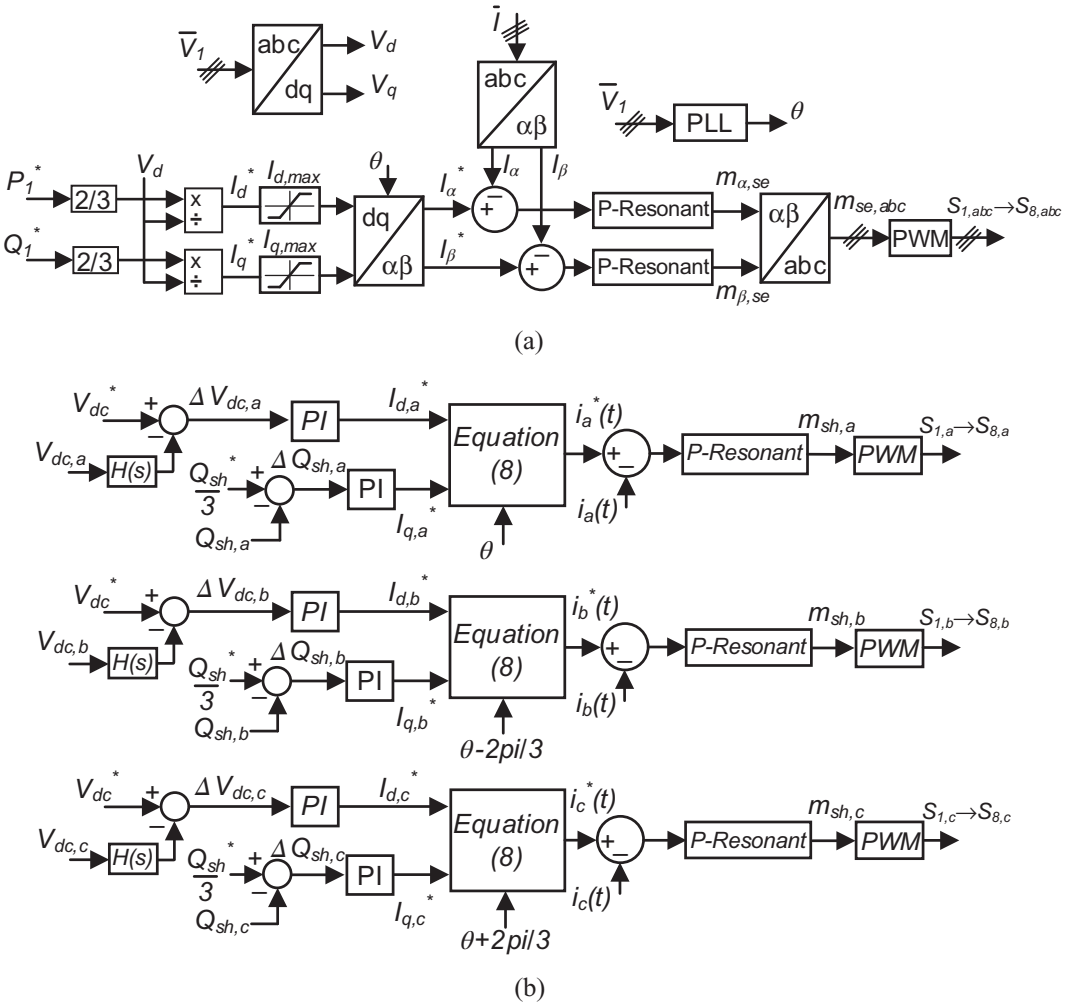

FIGURE 8 Control loops of the modified UPFC: (a) series converters and (b) shunt converters

4.3 | Second-order filter

The measured feedback DC voltage signal (i.e. $V_{dc,a}$, $V_{dc,b}$, and $V_{dc,c}$) has a DC voltage component and a ripple component. The ripple component is mainly double frequency harmonics that inherently exist with single-phase converters.

Second-order digital filters $H(s)$ are connected to the measured feedback voltage signals to extract the DC voltage components and prevent the ripple components from being introduced to the control loops, hence improving the control loops' performance. The transfer function $H(s)$ is given, as in (9).

$$H(s) = 1 - \frac{2\xi w_0 s}{s^2 + 2\xi w_0 s + {w_0}^2} \tag{9}$$

where w_0 and ξ are the desired double frequency harmonics and the damping factor. Using $w_0 = 200\pi$ and $\xi = 0.05$, the Bode diagram in Figure 9 was obtained and the magnitude (dB) shows that the transfer function provided very low gain around the resonant frequency $w_0 = 200\pi$.

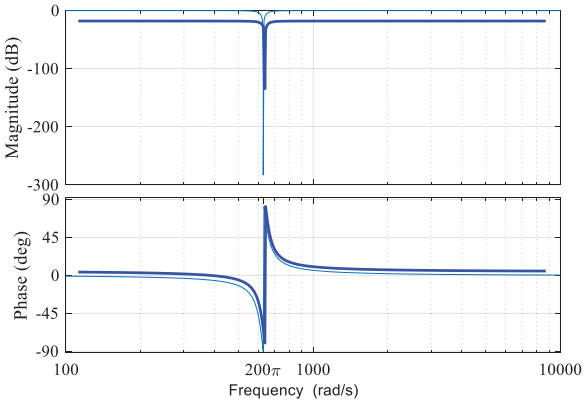

FIGURE 9 Bode diagram of second-order filter

5 | SIMULATION RESULTS

Figure 10 shows the case study used to conduct the simulation analysis. Figure 10a shows the modified UPFC model that was built in MATLAB Simulink using the switched representation of single-phase three-level NPC converters. Figures 10b and 10c

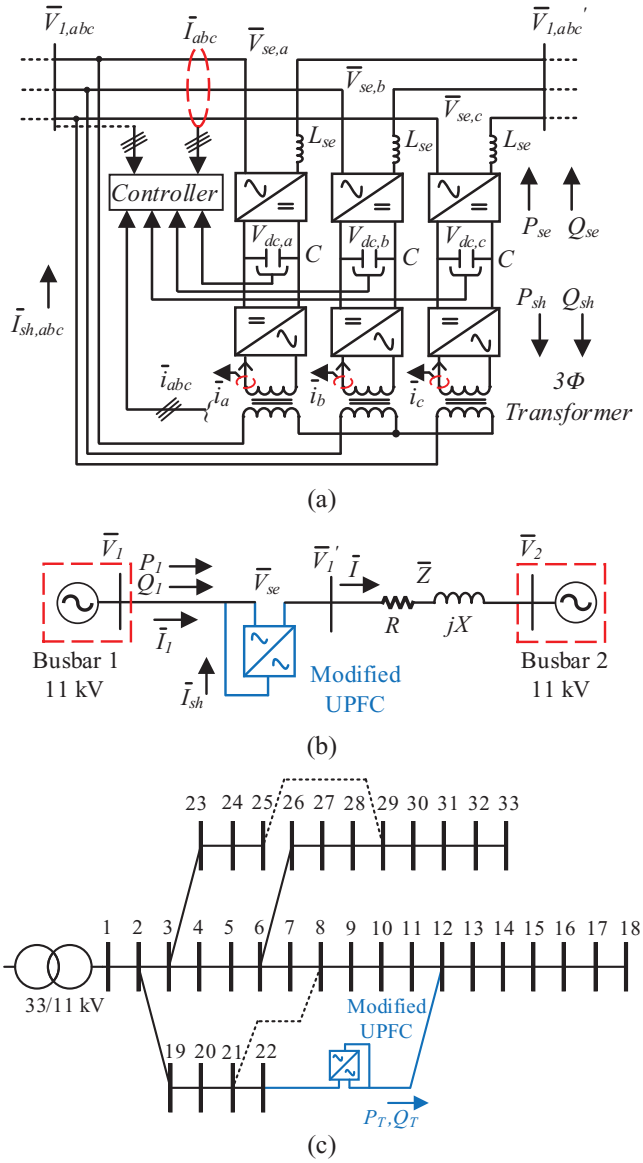

FIGURE 10 Case study implemented in Simulink: (a) modified UPFC model, (b) a two-busbar distribution network, and (c) the enhanced IEEE 33-bus distribution network [29]

show a two-busbar distribution network and the enhanced IEEE 33-bus benchmark distribution network used to test the performance of the modified UPFC by performing several step changes of active and reactive power and power flow reversal.

5.1 | A simple two-busbar distribution network

The modified UPFC was connected to an 11 kV, 5 MVA distribution feeder of a two-busbar distribution network as shown in Figure 10b. The impedance of the distribution feeder is 0.053 pu, X/R of 2.0. The base voltage and apparent power are 11 kV and 5 MVA. Referring to Section 3.1, the series voltage is approximately 10%. As a result, the series voltage $|\overline{V}_{se}|$ was considered 750 V (phase-voltage). Table 1 shows the parameters of the modified UPFC model shown in Figure 10a.

TABLE 1 Parameters of the modified UPFC model

Parameters	Value
Filter inductance, L_{se}	150 μH
DC capacitance, C	12 mF
DC-link voltage, V_{dc}	1,200 V
Rated power of series converter, S_{se}	630 kVA
Rated power of shunt converter, S_{sh}	630 kVA
Shunt transformer	11/1.6 kV, 630 kVA, Z_{tr} = 6%

The minimum DC voltage for a single phase VSC is obtained from $V_{ph,peak} = m\, V_{dc}$, where (m) is the modulation index. A 10% reserve voltage was considered together with the minimum DC voltage to ensure proper operation during transients and to consider the voltage drop across the interfacing impedance (e.g. series AC filter and shunt transformer) [30]. As $|\overline{V}_{se}| = 750$ V rms, then $V_{ph,peak} = \sqrt{2} \times 750$ and the maximum modulation index (m) of SPWM is 1.0, the DC voltage V_{dc} was selected to be 1,200 V.

The voltage rating of the IGBTs was selected such that the summation of the DC voltage, ripple voltage, and turn off overshoot voltage is restricted to 70% of IGBT's nominal voltage rating [30]. Given that the blocking voltage of the IGBTs is half of the DC voltage (i.e. 600 V) and the feeders' nominal power is 5 MVA, the Infineon IGBTs of 1.2 kV, 300 A (FF1800R17IP5BPSA1) were selected. The IGBT unit price is approximately 1,537£ [31]. Note that the series converters are vulnerable to immediate overvoltages and overcurrents during external faults. In [32], a protection circuit was proposed to bypass the series converter in a few milliseconds when external faults occur on the distribution network.

Several criteria should be considered when selecting a DC-link capacitor, such as capacitor technology (e.g. film and electrolytic), voltage rating, and current stresses [33]. The DC-link capacitance was calculated from $C \geq \frac{S_{1-ph}}{\omega\, V_{dc}\, \Delta V_{dc}}$ [34]. Given that $S_{1\text{-}ph}$ = 210 kVA, ΔV_{dc} = 4%, and V_{dc} = 1,200 V, the required DC-link capacitance is 12 μF. The DC-link capacitance can be achieved by a capacitor bank, for example, 10 capacitors in parallel and each of 1,290 μF and 1,300 V (WIMA DC-link MKP 6HP [35]). The weight of a single capacitor is approximately 4.3 kg and has a diameter of 116 mm and a height of 342 mm. The total weight and volume of the DC-link capacitors are 43 kg and 0.036 m^3. The DC-link capacitors do not burden the system too much, given that the 630 kVA interfacing shunt transformer has a weight and volume of approximately 1,900 kg and 2.12 m^3[18].

Figure 11 shows the response of the modified UPFC model to control signals to step change active and reactive power P_1 and Q_1 at 0.4 s, 0.8 s, and 1.2 s, and reverse P_1 and Q_1 at 1.6 s, 2.0, and 2.4 s. Figure 11a shows accurate and fast-tracking performance to P_1^* and Q_1^*. At t = 0.4 s, P_1 was increased to 4 MW, while Q_1 was maintained constant at 1 MVAr. At t = 0.8 s,

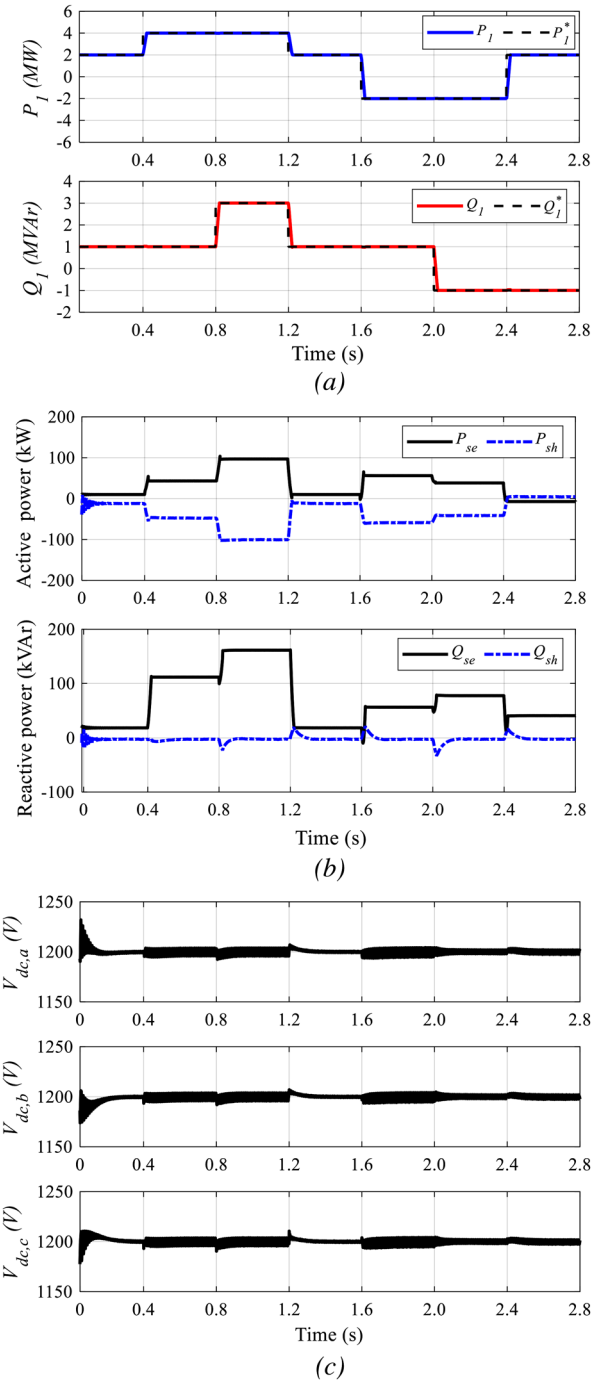

FIGURE 11 Response of the modified UPFC in a two-busbar network: (a) active and reactive power flow, (b) converters' active and reactive power, and (c) DC-link voltages

Q_1 was increased to 3 MVAr and the distribution feeder transferred its full capacity (i.e. 5 MVA). At $t = 1.2$ s, P_1 and Q_1 were decreased to 2 MW and 1 MVAr. At $t = 1.6$ s, P_1 was reversed to −2 MW, while Q_1 was maintained constant, then at $t = 2.0$ s, Q_1 was reversed to -1 MVAr, while P_1 was kept unchanged at −2 MW. At $t = 2.4$ s, P_1 was reversed to 2 MW, while Q_1 was maintained constant at −1 MVAr. These demonstrate the ability of the modified UPFC to independently control active and reactive power of the distribution feeder.

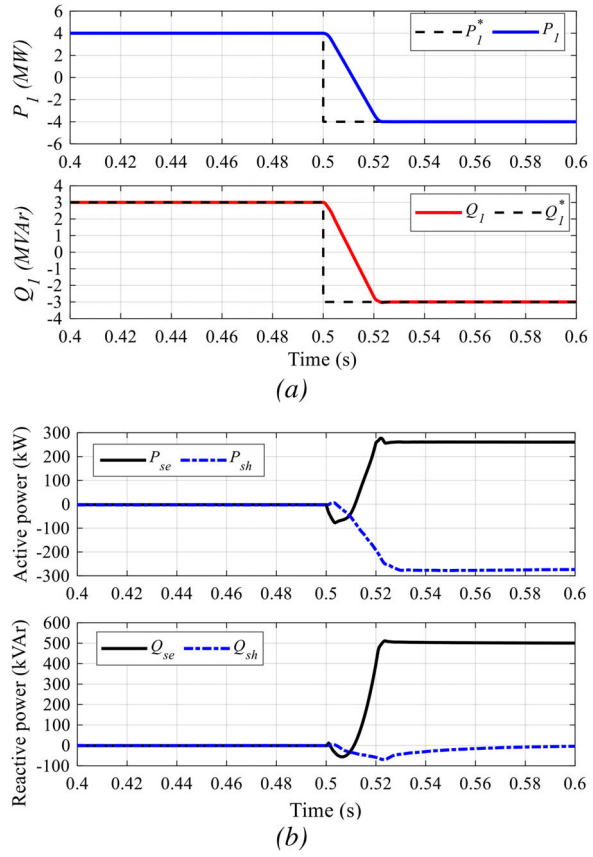

FIGURE 12 Active and reactive power reversal: (a) feeders' active and reactive power and (b) converters' active and reactive power

Figure 11b shows the active and reactive power of the series and shunt converters. The active power exchanged by the series converters approximately equals the active power of the shunt converters (i.e. $P_{se} + P_{sh} \approx 0$) in the steady-state, apart from the active losses absorbed to supply the converters' and the shunt transformer's internal losses. The series converters exchanged reactive power Q_{se}, while the reactive power of the shunt converters Q_{sh} was set to zero. Figure 11c shows that the DC voltage controllers well regulated the DC voltages of the DC-link buses.

Figure 12 shows power flow reversal of P_1 and Q_1 occurred at $t = 0.5$ s. Before $t = 0.5$ s, the uncompensated active and reactive power flow from busbar 1 to busbar 2 were 4 MW and 3 MVAr. After $t = 0.5$ s, the power flow was reversed to −4 MW and −3 MVAr as shown in Figure 12a. In this case, the controllable power was maximum (i.e. $\sqrt{P_c^2 + Q_c^2} = 2.0$pu).

Figure 12b shows active and the reactive power of the series and shunt converters. Before $t = 0.5$ s, the series and shunt converters exchanged zero active and reactive power. After $t = 0.5$ s, the series converters operated at its full capacity of apparent power and supplied active power of 261 kW and reactive power of 500 kVAr. The shunt converters absorbed 276 kW to supply the active power requested by the series converters, while no reactive power was provided at busbar $\overline{V}_1$ (i.e. $Q_{sh} = 0$).

Figure 13 shows the output voltage of the three single-phase series converters. Before $t = 0.5$ s, $|\overline{V}_{se}|$ was zero. After $t = 0.5$ s,

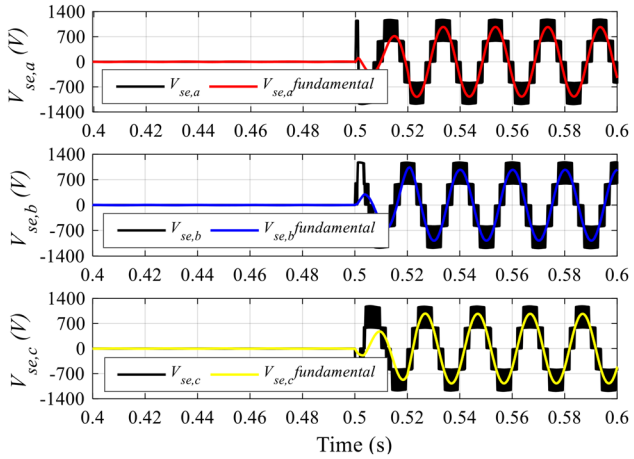

FIGURE 13 Maximum series voltage

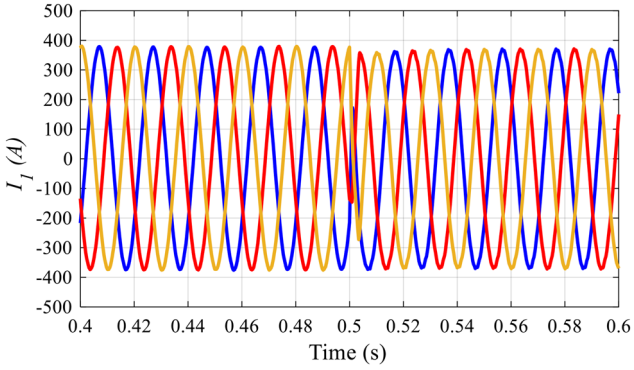

FIGURE 14 Current of Busbar 1 at full load

$|\overline{V}_{se}|$ was increased to 685 V phase-rms (i.e. $|\overline{V}_{se}| = 10.7\%$). Figure 14 shows current $\overline{I}_1$ of busbar 1 when the distribution feeder operated at full load with 262 A rms. The total harmonic distortion of the current $\overline{I}_1$ was 1.35%.

5.2 | Enhanced IEEE 33-bus distribution network

The enhanced IEEE 33-bus distribution network shown in Figure 10c was used to verify the performance of the modified UPFC in a benchmark distribution network. It has 33 buses and three looping branches (i.e. switchable tie lines). The network voltage is 11 kV, and the total active and reactive power of loads are 3.7 MW and 1.8 MVAr. The detailed parameters of the network are provided in [29]. The modified UPFC is used to regulate the power transfer between buses 12 and 22. The nominal power transfer is 1.2 MVA (i.e. $\sqrt{{P_T}^2 + {Q_T}^2} \leq 1.2$ MVA). The apparent power of the series, shunt converters, and shunt interfacing transformer of the modified UPFC are 150 kVA (i.e. 12.5% of 1.2 MVA).

Figure 15 shows the simulated performance of the modified UPFC in response to control signals to change active and reactive power P_T and Q_T between buses 12 and 22 of the enhanced IEEE 33-bus distribution network. Figure 15a shows accurate and fast-tracking performance to the reference active and reactive power ${P_T}^*$ and ${Q_T}^*$. Before $t = 0.4$ s, the modified UPFC regulated the power P_T and Q_T at 0.5 MW and 0.25 MVAr. After $t = 0.4$ s and 0.8 s, the power P_T and Q_T were independently increased to 1.0 MW and 0.5 MVAr, then decreased to 0.5 MW and 0.25 MVAr after $t = 1.2$ s and 1.6 s. After $t = 2.0$ s and

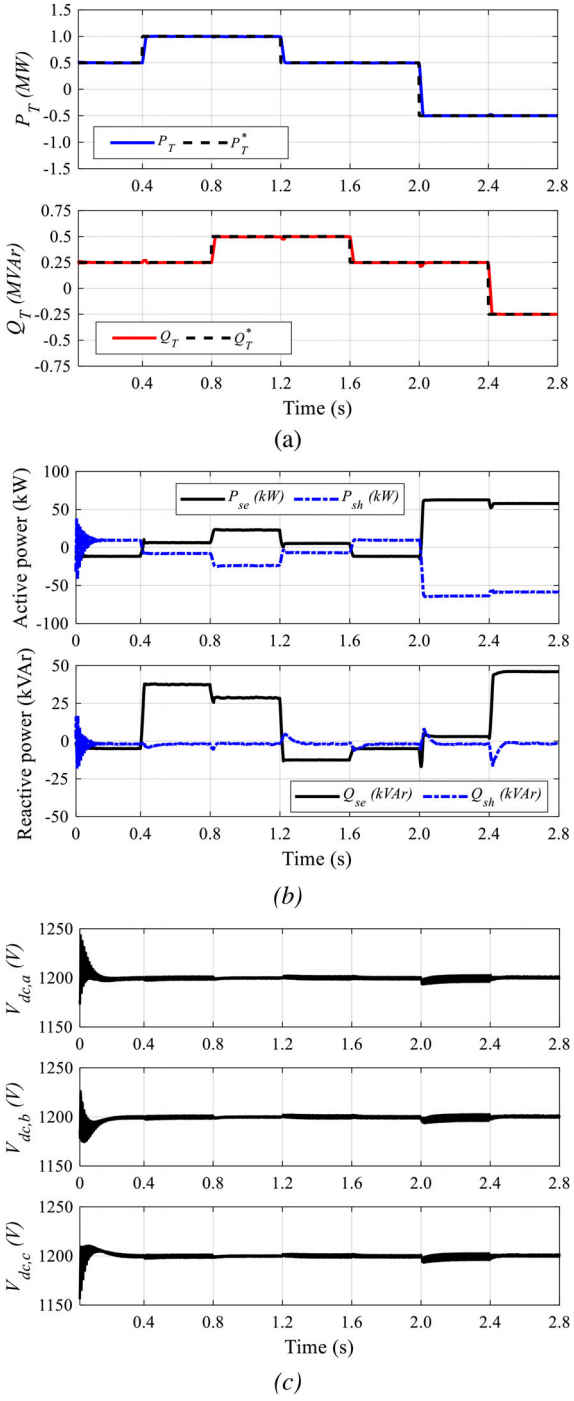

FIGURE 15 Response of the modified UPFC in the enhanced IEEE 33-bus network: (a) active and reactive power flow, (b) converters' active and reactive power, and (c) DC-link voltage

2.4 s, P_T and Q_T were reversed to −0.5 MW and -0.25 MVAr. Figure 15b shows the active and reactive power of the series and shunt converters. The series converters exchanged active and reactive power with the AC network. The shunt converters supplied/absorbed the active power requested by the series converter (i.e. $P_{se} \approx P_{sh}$). The reactive power of the shunt converters was set to zero ($Q_{sh} = 0$). Figure 15c shows the DC-link voltages. The DC-link voltages are well regulated to their reference values.

6 | CONCLUSION

The UPFC was modified for use in medium voltage distribution networks by eliminating the interfacing series transformer. The modified UPFC was built in MATLAB Simulink using the switched representation of single-phase three-level NPC converters and were controlled in power flow control mode. The single-phase series converters operated in the P–Q control scheme and regulated a distribution feeder's active and reactive power. The single-phase shunt converters operated in the V_{dc}–Q control scheme and maintained constant DC voltages. The control scheme provided an accurate and fast response during several step changes of active and reactive power and power flow reversal. The modified UPFC model demonstrated its capability to control the power flow of distribution networks using partially rated converters. Future work includes performing a cost–benefit analysis using single-phase and three-phase shunt converters.

ACKNOWLEDGEMENTS

The researcher Mohamed A. Abdelrahman is fully funded by Netwon-Mosharafa scholarship. This work was also supported in part by the Engineering and Physical Sciences Research Council, U.K., under Grant EP/T021969/1 and in part by Flexible Integrated Energy Systems (FLEXIS). FLEXIS is part-funded by the European Regional Development Fund (ERDF), through the Welsh Government under WEFO case 80836.

CONFLICT OF INTEREST

No conflict of interest to declare

DATA AVAILABILITY STATEMENT

Data sharing not applicable to this article as no datasets were generated or analysed during the current study

REFERENCES

1. Ofgem. Ofgem decarbonisation programme action plan. (2020). Accessed 10 Sep 2021
2. Carbon Plan. HM Government. https://assets.publishing.service.gov.uk/government/uploads/system/uploads/attachment_data/file/47621/1358-the-carbon-plan.pdf Accessed 14 Sep 2021
3. National Grid. Summer outlook report 2018. (2018). Accessed 9 Sep 2020
4. EA Technology. Review of GB Innovation strategies and Projects. (2016). Accessed 10 Oct 2020
5. Electricity NIC Initial Screening Submission 2019 – 'DC Share' (WPD). Ofgem. https://www.ofgem.gov.uk/publications/electricity-nic-initial-screening-submission-2019-dc-share-wpd Accessed 24 Oct 2021
6. Network Innovation Competition 2017 Submission. LV Engine. https://www.ofgem.gov.uk/system/files/docs/2017/11/lv_engine_2017_nic_full_resubmission_-_clean_redacted.pdf Accessed 28 Nov 2019
7. UK Power Networks Innovation – Active Response. https://innovation.ukpowernetworks.co.uk/projects/active-response/ Accessed 24 Oct 2021
8. ABB Advanced Power Electronics Grid intertie converter with extended STATCOM functionality, Sorowako (South Sulawesi), Indonesia. https://library.e.abb.com/public/d20bc6e606717f9bc12576c40043ea95/PCS%206000%20STATCOM_INCO_EN.pdf Accessed 24 Oct 2021
9. Bathurst, G., Hwang, G., Tejwani, L.: MVDC-the new technology for distribution networks. In: 11th IET International Conference on AC and DC Power Transmission, Birmingham, UK, 10–12 February 2015. https://doi.org/10.1049/CP.2015.0037
10. Liu, Y., Cao, X., Fu, M.: The upgrading renovation of an existing XLPE cable circuit by conversion of AC line to DC operation. IEEE Trans. Power Deliv. 32(3), 1321–1328 (2017) https://doi.org/10.1109/TPWRD.2015.2496178
11. Long, C., Wu, J., Thomas, L., Jenkins, N.: Optimal operation of soft open points in medium voltage electrical distribution networks with distributed generation. Appl. Energy 184, 427–437 (2016) https://doi.org/10.1016/j.apenergy.2016.10.031
12. Li, P., Ji, H., Wang, C., Zhao, G., Song, G., Ding, F., Wu, J.: Coordinated control method of voltage and reactive power for active distribution networks based on soft open point. IEEE Trans. Sustain. Energy 8(4), 1430–1442 (2017)
13. Bloemink, J., Green, T.C.: Benefits of distribution-level power electronics for supporting distributed generation growth. IEEE Trans. Power Deliv. 28(2), 911–919 (2013) https://doi.org/10.1109/TPWRD.2012.2232313
14. Abdelrahman, M., Long, C., Wu, J., Jenkins, N.: Optimal operation of multi-terminal soft open point to increase hosting capacity of distributed generation in medium voltage networks. In: 53rd International Universities Power Engineering Conference (UPEC), Glasgow, 4–7 September 2018. https://doi.org/10.1109/UPEC.2018.8541861
15. Schauder, C., et al.: AEP UPFC project: Installation, commissioning and operation of the ±160 MVA STATCOM (phase I). IEEE Trans. Power Deliv. 13(4), 1530–1535 (1998), https://doi.org/10.1109/61.714855
16. Kim, S., Yoon, J., Chang, B., Baek, D.: The operation experience of KEPCO UPFC. In: International Conference on Electrical Machines and Systems, Nanjing, China, September 2005, vol. 3, pp. 2502–2505. IEEE, New Jersey, United States. https://doi.org/10.1109/icems.2005.203026
17. Wang, X., et al.: Application of 500 kV UPFC in Suzhou southern power grid. IET Int. Conf. AC and DC Power Transmission (ACDC). 2019(16), 2580–2584 (2019) https://doi.org/10.1049/joe.2018.8556
18. Huber, J., Kolar, J.: Volume/weight/cost comparison of a 1MVA 10 kV/400 V solid-state against a conventional low-frequency distribution transformer. In: IEEE Energy Conversion Congress and Exposition, Pittsburgh, PA, September 2014, pp. 4545–4552. IEEE, New Jersey, United States. https://doi.org/10.1109/ECCE.2014.6954023
19. Trihal-dry type distribution transformer. Schneider Electric. https://www.se.com/au/en/product-range/977-trihal/?parent-subcategory-id=3610&filter=business-6-medium-voltage-distribution-and-grid-automation Accessed 26 Feb 2022
20. Jijun, Y., Haiqing, X., Jiankun, L.,Gang, C., Qun, L., Peng, L.: Unified power flow controller technology and application. Science Direct (2017). https://www.sciencedirect.com/book/9780128134856/unified-power-flow-controller-technology-and-application#book-info
21. Bottrell, N., Terry, S., Ash, N., Grella, L.: Active response to distribution network constraints. In: 25th International Conference on Electricity Distribution, Cired, Madrid, 3–6 June 2019
22. Teichmann, R., Bernet, S.: A comparison of three-level converters versus two-level converters for low-voltage drives, traction, and utility applications. IEEE Trans. Ind. Appl. 41(3), 855–865 (2005) https://doi.org/10.1109/TIA.2005.847285
23. MV7000, Medium Voltage Drives, GE Power Conversion. https://www.gepowerconversion.com/product-solutions/medium-voltage-drives/mv7000 Accessed 16 Nov 2020

24. Lee, S., Lee, J., Lee, K.: Novel switching strategy for high-efficiency of single-phase three-level inverters. In: IEEE Conference on Energy Conversion (CENCON), Johor Bahru, Malaysia, September 2014, pp. 342–347. IEEE, New Jersey, United States. https://doi.org/10.1109/CENCON.2014.6967527
25. Kuperman, A.: Proportional-resonant current controllers design based on desired transient performance. IEEE Trans. Power Electron. 30(10), 5341–5345 (2015), https://doi.org/10.1109/TPEL.2015.2408053
26. Busarello, T., Pomilio, J., Simoes, M.: Design procedure for a digital proportional-resonant current controller in a grid connected inverter. In: 4th IEEE Southern Power Electronics Conference (SPEC), Santos, Brazil, 1–4 Dec 2019. https://doi.org/10.1109/SPEC.2018.8636052
27. Holmes, D., Lipo, T., McGrath, B., Kong, W.: Optimized design of stationary frame three phase AC Current regulators. IEEE Trans. Power Electron. 24(11), 2417–2426 (2009), https://doi.org/10.1109/TPEL.2009.2029548
28. McGrath, B., Holmes, D., McNabb, L.: A signal conditioning antiwindup approach for digital stationary frame current regulators. IEEE Trans. Ind. Appl. 55(6), 6036–6046 (2019), https://doi.org/10.1109/TIA.2019.2929144
29. Dolatabadi, S.H., Ghorbanian, M., Siano, P., Hatziargyriou, N.D.: An enhanced IEEE 33 bus benchmark test system for distribution system studies. IEEE Trans. Power Syst. 36(3), 2565–2572 (2021), https://doi.org/10.1109/TPWRS.2020.3038030
30. Marzoughi, A., Burgos, R., Boroyevich, D., Xue, Y.: Design and comparison of cascaded H-bridge, modular multilevel converter, and 5-L Active neutral point clamped topologies for motor drive applications. IEEE Trans. Ind. Appl. 54(2), 1404–1413 (2018) https://doi.org/10.1109/TIA.2017.2767538
31. FF1800R17IP5BPSA1-Infineon Technologies. DigiKey, https://www.digikey.com/en/products/detail/infineon-technologies/FF1800R17IP5BPSA1/7791797 Accessed 3 Mar 2022
32. Bashar, E., et al.: A new protection scheme for an SSSC in an MV network by using a varistor and thyristors. IEEE Trans. Power Deliv. 36, 102–113 (2020) https://doi.org/10.1109/TPWRD.2020.2982512
33. Domingues-Olavarria, G., Fyhr, P., Reinap, A., Andersson, M., Alakula, M.: From chip to converter: a complete cost model for power electronics converters. IEEE Trans. Power Electron. 32(11), 8681–8692 (2017), https://doi.org/10.1109/TPEL.2017.2651407
34. Neumayr, D.: The essence of the little box challenge – part A: key design challenges & solutions. CPSS Trans. Power Electron. Appl. 5(2), 158–179 (2020) https://doi.org/10.24295/CPSSTPEA.2020.00014
35. DC-link capacitors. WIMA DC-Link MKP 6 HP. https://www.wima.de/en/our-product-range/dc-link-capacitors/ Accessed 18 Feb 2022

How to cite this article: Abdelrahman, M.A., Yang, P., Ming, W., Wu, J., Jenkins, N.: Modified unified power flow controller for medium voltage distribution networks. IET Gener. Transm. Distrib. 1–11 (2022). https://doi.org/10.1049/gtd2.12567